Supplementary Materials for

In situ architecture, function, and evolution of a contractile injection system

Désirée Böck, João M. Medeiros, Han-Fei Tsao, Thomas Penz, Gregor L. Weiss, Karin Aistleitner, Matthias Horn, Martin Pilhofer

This PDF file includes:

Other Supplementary Materials for this manuscript includes the following:

Materials and Methods

Cell cultures

Acanthamoeba castellanii strain 5a2 (ATCC PRA-228) and *Acanthamoeba castellanii* 5a2 infected with *Amoebophilus asiaticus* strain 5a2 (DSMZ 27557) were cultivated using 10 mL Trypticase-Soy-Yeast (TSY) extract broth (30 g/L Trypticase soy broth, 10 g/L Bacto Yeast extract). Cultures were incubated at 27°C and passaged every 5 to 10 days. Growth of the cultures was regularly monitored by light microscopy.

Purification of amoebophili

To purify intracellular amoebophili, infected amoebae were homogenized using a Dounce tissue grinder (Wheaton). The amoeba lysate was filtered (5 µm pore size) to separate intact amoebae and cell debris from amoebophili. The filtrate was centrifuged (5000×g, 6 min) and the pellet was resuspended in TSY medium. Extracellular amoebophili were harvested from infected cultures by filtering (5 µm pore size) the supernatant of the amoebae culture and pelleting the filtrate (5000×g, 6 min).

Quantification of amoebae and purified amoebophili

Amoebae were counted in a Neubauer haemocytometer using an inverse phase contrast microscope (10x objective, no immersion). High-density cultures were first diluted for accurate counting. For bacterial quantification, the *Amoebophilus* suspension was diluted in 1×Page's amoebic Saline (20 mM NaCl, 0.16 mM MgSO4 • 7 H20, 0.27 mM CaCl2 • 2 H20, 10 mM Na2HPO4, 10 mM KH2PO4) and vacuum filtered, first using a cellulose acetate membrane support filter (0.45 µm), and then a black polycarbonate membrane filter (0.22 µM). Bacterial cells on the polycarbonate filter were stained with DAPI (4',6-diamidino-2-phenylindole) (1 µL/mL) for 5 min in the dark. The polycarbonate membrane was transferred to a standard microscope slide for counting 10-15 random spots.

Infection of amoebae with amoebophili

For infection experiments, non-infected amoebae were seeded into culture flasks. For early time points (1 hpi, 2 hpi), 10^6 amoebae were seeded and infected at an MOI of 5000. For later time points (72 hpi, 144 hpi), 5×10^5 amoebae were infected at an MOI of 500. To stimulate and synchronize the infection, culture flasks were centrifuged at 300×g for 10 min after the addition of amoebophili. Cultures were incubated at 27°C. All experiments were performed in three biological replicates with three technical replicates each.

For electron microscopy (EM) imaging experiments, EM finder grids (gold NH2 R2/2, Quantifoil) were sterilized under UV light and then glow discharged. Grids were placed on the bottom of the wells of a 12-well plate (Nunc, Thermofisher) and equilibrated with TSY medium. The infection was performed as described above.

Visualization of infection by fluorescence in situ hybridization

Bacterial infection was monitored by fluorescence in situ hybridization (FISH) (*25*). Cells were identified and quantified by using three different probes. Probes EUK516-Cy5

and Aph1180-Cy3 are specific for eukaryotes and *Amoebophilus*, respectively (*10*, *26*). Additionally, an unspecific bacterial probe (EUB338-Fluos) (*26*) was used to identify potential bacterial contaminations. A 2 mL aliquot of the infected amoeba culture was centrifuged (5000×g, 6 min, 20°C). The pellet was resuspended in 60-200 µL sterile 1×PAS. Amoebae were seeded onto the wells of a Teflon-coated microscope slide and fixed with 4 % PFA (paraformaldehyde) after attachment. Each well was incubated with 10 µL hybridization buffer (5 M NaCl, 1 M Tris-HCl, 20 % formamide, 1 % SDS), containing 1 µL of each probe. Microscope slides were incubated at 46°C in a closed and hybridization buffer-saturated environment in the dark for 90-120 min. Slides were washed with prewarmed (48°C) washing buffer (5 M NaCl, 1 M Tris-HCl, 0.5 M EDTA) followed by double distilled water (ddH20) (4°C). Slides were dried with compressed air and analyzed using a white light laser confocal microscope (Leica TCS SP8 X). Image analysis was performed using the Leica software LAS AF version 3.2.1.9702.

Quantification of *Amoebophilus* infectivity and intracellular survival

Extracellular amoebophili were purified as described above. Intracellular amoebophili were harvested from a synchronized amoeba culture at 96 hpi. *Amoebophilus* cells were quantified as described above. Non-infected amoebae were seeded into culture flasks. For all time points (1 and 4 hpi), 10^6 amoebae were seeded and infected at an MOI of 4000 with either intra- or extracellular amoebophili. To stimulate and synchronize the infection, culture flasks were centrifuged at 300×g for 12 min after the addition of amoebophili. Cultures were subsequently incubated at 27°C. After 40 min cultures were washed with TSY medium to remove non-internalized amoebophili. Cells were fixed at 1 and 4 hpi and subjected to FISH analysis (see above). 300-800 randomly chosen amoebae were analysed for the presence or absence of intracellular amoebophili (as a measure for infectivity and intracellular survival). All experiments were performed in quadruplicates. Data were analyzed by the Student's t-test (two-sided) with Welch's correction. Data are displayed as mean and standard deviation.

Quantification of sheath transcripts

RNA was isolated from infected amoeba cultures (at 12, 68 and 140 hpi), from extracellular amoebophili, and from non-infected amoebae. Extracellular amoebophili were harvested as described above and amoeba cells were harvested by centrifugation (8000×g, 2 min). Pellets were resuspended in 750 µL TRIzol (Life Technologies). The cell suspension was transferred to a Lysing Matrix A Tube (MP Biomedicals) and homogenized using a BIO101/Savant FastPrep FP120 instrument (speed: 4.5 m/sec, 30 sec). RNA was extracted per manufacturer's recommendations (TRIzol, Life Technologies). Remaining DNA was removed using the TURBO DNA-free Kit (Ambion). After DNase treatment, RNA was dissolved in ddH2ODEPC (0.1 % v/v) and stored at -80°C. The absence of DNA contamination was verified by a control PCR targeting a 141 bp fragment of Aasi_1074. All RNA isolates were performed in triplicates.

Real time quantitative polymerase chain reaction (RT-qPCR) was performed according to the MIQUE guidelines (*27*). For first strand cDNA synthesis, reverse transcription was performed with 500 ng total RNA, random hexamers, and SuperScript

III Reverse Transcriptase (Life Technologies). Samples from each infection time point were subjected to reverse transcription (50°C, 60 min). A total volume of 25 µL was used for each technical triplicate. RT-qPCR was performed using a CFX96Touch Real-time PCR Detection System (Bio-Rad, Hercules, CA) with primers targeting a 141 bp fragment of the sheath gene (Aasi_1074 qPCR F1: 5'-GTGGTGCAGATTGCTACATCAT-3'; Aasi_1074 qPCR R1: 5'-AGTCGGGCATAAGCAACATAGT-3'). Primers targeting a 167 bp fragment of an RNA polymerase gene (Aasi_1396) were used for normalization (Aasi_1396 qPCR F2: 5'-ACTAGGTACGCCACCTGAAAAA-3'; Aasi_1396 qPCR R2: 5'-AAGTTACTCCCCTTTCCACACA-3'). Primers were used at a final concentration of 200 nM. RT-qPCR reactions were prepared using the iQ SYBR Green Supermix (BioRad). Reaction conditions were optimized with genomic DNA isolated from a continuous culture of infected amoebae. The following parameters were used for all RT-qPCR reactions: initial denaturation step at 95°C for 3 min, followed by 45 cycles of denaturation at 95°C for 30 sec, annealing at 65.7°C for 30 sec, and elongation at 72°C for 30 sec. To assess the specificity of the amplification, a melting curve starting at 55°C was recorded. The temperature was increased incrementally by 0.5°C every 10 sec until the final temperature of 95°C. Standard curves were obtained for both genes using TOPO XL plasmids (Life Technologies) containing a 1507 bp insert of Aasi_1074 and a 851 bp fragment of Aasi_1396. RT-qPCR standards were quantified using Quant-IT PicoGreen ds Assay Kit (Life Technologies). The amount of DNA in DNase-treated RNA was determined by performing RT-qPCR reactions with DNase-treated RNA from different infection samples. Additionally, a no-target control (cDNA from non-infected amoebae) and a no-template control (reverse transcription with water) were included in all RT-qPCR assays to ensure the specificity of the assay. Data were analyzed using the CFX Manager (v 2.1, BioRad). The mean starting quantity (SQ) was calculated from qPCR standards. Aasi_1074 mRNA levels from each time point were calculated as ratios relative to 68 hpi.

Sheath purification and protein identification

Extracellular amoebophili purified from 250 mL culture supernatant were pelleted, resuspended in 3 mL lysis buffer (150 mM NaCl, 50 mM Tris-HCl, 0.5×CellLytic B [Sigma-Aldrich], 1 % Triton X-100, 200 µg/mL lysozyme, 50 µg/mL DNAse I, 1 mM phenylmethylsulfonyl fluoride [PMSF], pH 7.4), and incubated for 10 min at 37°C. Samples were stored at 4°C until centrifugation (15000×g, 15 min, 4°C). Cleared lysates were subjected to ultra-centrifugation (150000×g, 1 h, 4°C) and pellets were resuspended in 400 µL resuspension buffer (150 mM NaCl, 50 mM Tris-HCl, 22 µL protease inhibitor cocktail [PIC], pH 7.4). Proteins in the sheath preparation were identified by mass spectrometry at the Functional Genomics Center Zürich.

Preparation of frozen-hydrated specimens

Plunge freezing was performed according to Weiss et al. (*28*). Purified *Amoebophilus* cells or sheath preparations were mixed with 10 nm BSA-coated colloidal gold particles (1:4 v/v, Sigma). A 4 µL droplet of the mixture was applied to a glow-discharged copper EM grid (R2/2, Quantifoil). The grid was automatically blotted from both sides and plunge-frozen in liquid ethane-propane (37 %/63 %) using a Vitrobot (FEI

Company). Grids that were incubated in amoebae cultures were removed from the well using forceps. The forceps was mounted in the Vitrobot and the grid was blotted only from the backside by installing a Teflon sheet (instead of filter paper) on one of the blotting pads. Grids were stored in liquid nitrogen.

Cryo-focused ion beam milling

Cryo-focused ion beam (cryo-FIB) milling was used to prepare samples of plunge-frozen amoebae that could then be imaged by electron cryotomography (*15*). Frozen grids with infected amoeba cells were transferred into the liquid nitrogen bath of a loading station (Leica Microsystems) and clamped onto a "40° pre-tilted TEM grid holder" (Leica Microsystems). The holder with grids was shuttled from the loading station to the dual beam instrument using the VCT100 transfer system (Leica Microsystems). The holder was mounted on a custom-built cryo-stage in a Helios NanoLab600i dual beam FIB/SEM instrument (FEI). The stage temperature was maintained below -154°C during loading, milling and unloading procedures. Grid quality was checked by scanning EM (SEM) imaging (5 kV, 21 pA). The samples were then coated with a Platinum (Pt) precursor gas using the Gas Injector System. We adapted a "cold deposition" technique (*29*) that was published previously (needle distance to target of 8 mm, temperature of the precursor gas of 27 °C, and open valve time of 6 s). Lamellae were milled in several steps. We first targeted two rectangular regions to generate a lamella with ~2 µm thickness with the ion beam set to 30 kV and ~400 pA. The current of the ion beam was then gradually reduced until the lamella reached a nominal thickness of ~350 nm (ion beam set to ~25 pA). Up to 8 lamellae were milled per grid. After documentation of the lamellae by SEM imaging, the holder was brought back to the loading station using the VCT100 transfer system. The grids were unloaded and stored in liquid nitrogen.

Electron cryomicroscopy and electron cryotomography

Sheath preparations, purified *Amoebophilus* cells and cryo-FIB processed infected amoebae were examined by electron cryomicroscopy and electron cryotomography (ECT)(*28*). Images were recorded on a Tecnai Polara TEM (FEI) equipped with post-column GIF 2002 imaging filter and K2 Summit direct electron detector (Gatan), or on a Titan Krios TEM (FEI) equipped with a Quantum LS imaging filter and K2 Summit (Gatan). Both microscopes were operated at 300kV and the imaging filters with a 20 eV slit width. The pixel size at the specimen level ranged from 5.95 Å to 3.45 Å. Tilt series covered an angular range from -60° to +60° with 1° (whole cells) or 2° (lamellae, sheath preparations) increments and -5 to -8 µm defocus. The total dose of a tilt series was 150 $e^-/Å^2$ (whole cells), 120 $e^-/Å^2$ (FIB-milled lamellae), or 100 $e^-/Å^2$ (sheath preparations). Tilt series and 2D projection images were acquired automatically using UCSF Tomo (*30*) or SerialEM (*31*). Three-dimensional reconstructions and segmentations were generated using the IMOD program suite (*32*).

Sub-tomogram averaging

Tomograms used for subtomogram averaging of the extended conformation were CTF-corrected in IMOD. Extended and contracted sheath structures were identified visually in individual tomograms and their longitudinal axes were modeled with open contours in 3dmod (*32*). Model points, the initial motive list, and the particle rotation

axes were generated using the stalkInit program from the PEET package (*33*). This approach allowed the definition of each structure's longitudinal axis as the particle y-axis. For the extended conformation, 243 individual structures were averaged using PEET with a box size of 34 pixels (x) by 34 pixels (z) by 150 pixels (y), at a pixel size of 0.81 nm. For the contracted conformation, 183 contracted structures were averaged with a box size of 28 pixels (x) by 28 pixels (z) and 86 pixels (y), at a pixel size of 1.38 nm. A random particle was chosen as a first reference and PEET's missing wedge compensation was activated. After analyzing the resulting average of the extended conformation, rotational 3-fold, 5-fold and 6-fold symmetries were imposed with a box size of 40 pixels (x) by 40 pixels (z) by 150 pixels (y). The contracted average was symmetrized 6-fold. Fourier shell correlation curves were calculated in PEET to estimate resolution. A hexagonal prism mask centered on the structures' longitudinal axes was applied to the volumes using imodmop (IMOD package) in order to mask neighboring structures for visualization purposes. UCSF Chimera (*34*) was used for visualization of the 3D models. 3-fold symmetric components were identified by manual assessment of the C3-symmetrized volume and their positions were excised by masking the surrounding densities with imodmop (fig. S2). The overlay (fig. 2B) of the extended conformation average with the T4 structure was produced in Chimera. The T4 model of the minimal composition of a contractile injection system was obtained from N. Taylor (*13*). In order to convey the connections between neighboring structures (fig. 2J/K), seven copies of a 3D model of a masked extended average were segmented and positioned in Chimera. The "morph map" function in Chimera was used to produce movie S6.

Hemolytic activity assay

A 10 µL aliquot of the bacterial suspension (9.1×10^8 bacteria) was mixed with 100 µL PBS and 190 µL of a 2 % (v/v) sheep erythrocyte suspension (Oxoid). *E. coli* BL21 and DH5α were used as negative control organisms, and *S.* Typhimurium SL1344 was used as a positive control organism. *Amoebophilus* control samples for imaging by ECT were incubated only with PBS and treated identically to all other samples. Samples were incubated for 1 h at 37°C on an orbital shaker (150 rpm). Plates were centrifuged (500×g, 5 min, 20°C) and a 100 µL aliquot of each well was transferred into a new 96-well-plate. The optical density of the supernatants was measured at 395 nm, 410 nm, 540 nm and 595 nm, to assess the degree of hemolysis (*35*, *36*). Negative (erythrocytes with PBS) and positive (erythrocytes with Triton X-100) assay controls were included in all experiments. Cytotoxicity was scored as percentage of cell lysis of the positive assay control (Triton X-100). All data points were blanked to the negative assay control to exclude false positive results due to spontaneous hemolysis. Data are expressed as mean and standard deviation of at least three independent experiments. Data were analyzed by the Student's t-test (two-sided) with Welch's correction.

Immunological detection of Hcp secretion

Hexahistidine-tagged Hcp (full length) and sheath (1-400 amino acids) proteins were recombinantly expressed in *E. coli* BL21 and affinity-purified (GenScript, USA). New Zealand Rabbits were immunized (standard polyclonal antibody protocol) and affinity-purified (GenScript, USA).

Aliquots of extracellular amoebophili were pelleted (5000×g, 6 min) and denatured (95°C, 10 min). Samples containing secreted Hcp were first subjected to TCA (trichloroacetic acid) precipitation (20 % TCA), then resuspended in Laemmli buffer (4×), and incubated for 10 min at 95°C. A 20 µL aliquot of each sample was loaded onto a 12 % SDS-PAGE gel. Proteins were transferred to a nitrocellulose membrane (Amersham) and blocked (5 % skim milk powder, 0.05 % Tween 20) for 1 h. Hcp was detected with polyclonal rabbit anti-Hcp antibodies (1:850 in PBS, 2 % skim milk, 0.05 % Tween 20) in combination with horseradish peroxidase-conjugated goat anti-rabbit IgG (Abcam) and a chemiluminescent substrate (ECL, Amersham). To exclude false positive results from intracellular Hcp released by accidental/occasional bacterial cell lysis, polyclonal rabbit anti-sheath antibodies were used as a marker for non-secreted cytoplasmic proteins (1:1000 in PBS, 2 % skim milk, 0.05 % Tween 20).

Immunogold labeling

Purified sheath was loaded onto copper EM grids (Formvar) and incubated for 5 min (20°C). Sheaths were fixed in 4 % PFA for 15 min (20°C). EM grids were subsequently quenched in 0.05 M glycine/PBS for 15 min (20°C). Samples were blocked in blocking buffer (5 % BSA/0.1 % gelatin in PBS; Sigma) for 1 h at 20°C. Grids were washed 3 × 5 min with blocking buffer followed by incubation with anti-sheath antibodies (1 h, 20°C). Next, EM grids were washed 6 × 5 min with blocking buffer before treatment with an anti-rabbit gold-conjugated (15 nm) secondary antibody (1 h, 20°C). Grids were washed 6 × 5 min with blocking buffer and 3 × 5 min with PBS. As a negative control, one reaction was processed without primary antibody. Grids were subsequently negatively stained (2 % tungsten). Micrographs were recorded on a Morgagni transmission electron microscope (FEI) operated at 80 keV.

Sequence analyses

Genomes for *Amoebophilus asiaticus* strain 5a2, *Cardinium hertigii* strain cEper1, *Serratia entomophila* plasmid pADAP, *Pseudoalteromonas luteoviolacea* strain HI1, *Francisella tularensis* strain SCHU S4, *Vibrio cholera* O1 biovar El Tor strain Inaba, *Pseudomonas aeruginosa* strain PAO1, *Flavobacterium johnsoniae* UW101, *Bacteroides fragilis* NCTC 9343, R-type bacteriocins of *P. aeruginosa*, and *Enterobacteria* phages T4 and P2 were downloaded from the NCBI Genome database. *Amoebophilus* nucleotide and amino acid sequences were used for BLASTN and BLASTP searches against the above-mentioned organisms. Protein sequences were analyzed using the HHpred server for protein homology detection (*37*). The PDB and Pfam databases were used to identify conserved protein domains. Protein hits were evaluated based on E-value, probability and secondary structure similarity. Only proteins showing the highest scores in these categories were considered as homologous.

Phylogenetic analyses

The phylogenetic relationships between contractile injection systems were examined by calculating phylogenetic trees using the sheath, tube and gp25 protein, respectively. Amino acid sequences were aligned in MEGA6 (*38*) using MUSCLE. Standard parameters were applied for multiple sequence alignments. Phylogenetic trees were reconstructed using the Maximum Likelihood (ML) method in MEGA6. Bootstrap values

(1000 resamples) were calculated to assess the robustness of the tree. Additionally, phylogenetic trees were calculated using the Neighbor joining (NJ), Maximum Parsimony, Minimum-Evolution and UPGMA method to confirm the topology of ML trees. Alignments and phylogenetic trees were also validated using MSAProbs (*39*) and the UPGMA method in PHYLIP-NEIGHBOR (*40*).

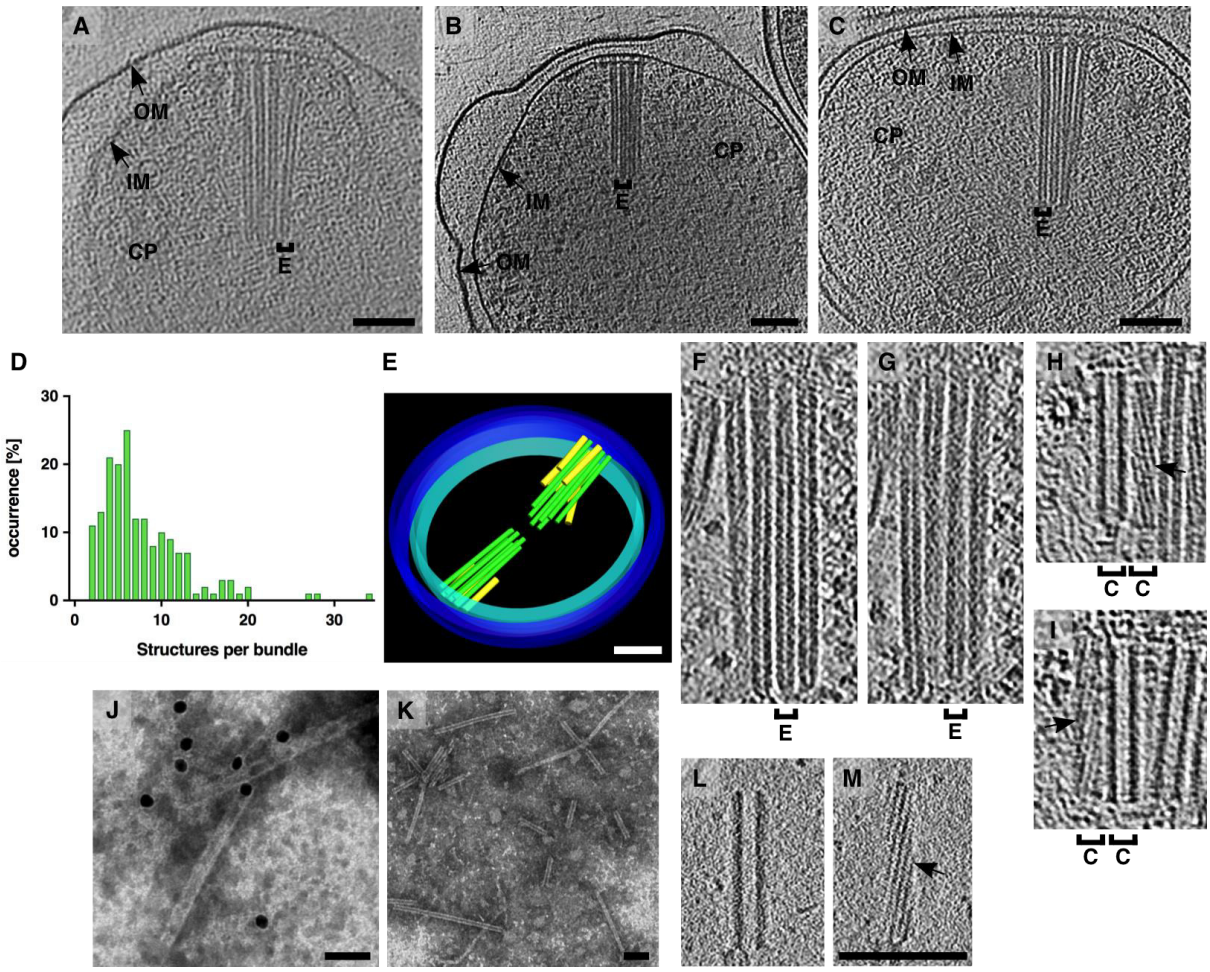

Fig. S1: Further characterization of *Amoebophilus* T6S-like structures.
(**A-C**) Examples of three additional *Amoebophilus* cells with bundles of contractile structures. Shown are 19-nm cryotomographic slices. "CP", cytoplasm; "E", extended T6SS; "IM", inner membrane; "OM", outer membrane. (**D**) Graph showing the distribution of structures per bundle. On average, bundles consisted of 8 structures (n=171 bundles). (**E**) Model of another example of an *Amoebophilus* cell harboring two almost opposed bundles (the average angle was 166°±17). Blue, outer membrane; cyan, inner membrane; green, extended T6SS; yellow, contracted T6SS. (**F-I**) Tomographic longitudinal (13-nm) slices (at different Z-heights) of intracellular extended (F/G, "E") and contracted (H/I, "C") T6S structures, showing differences in diameter, length and surface properties. Black arrows indicate helical ridges of contracted structures. (**J/K**) Negative stain EM images of an immunostaining of purified sheath with an Aasi_1074-specific primary antibody and gold-labeled secondary antibody. While gold-staining of sheaths was observed in the sample processed with both primary and secondary antibodies (J), the control (K, no primary antibody) did not show any gold labels associated with sheath structures. (**L/M**) Central (L) and top (M) slices (4 nm) through a cryotomogram of purified sheath. Note the structural similarities with the contracted structures observed in situ (H/I). Bars: 100 nm (F-I, L/M to scale).

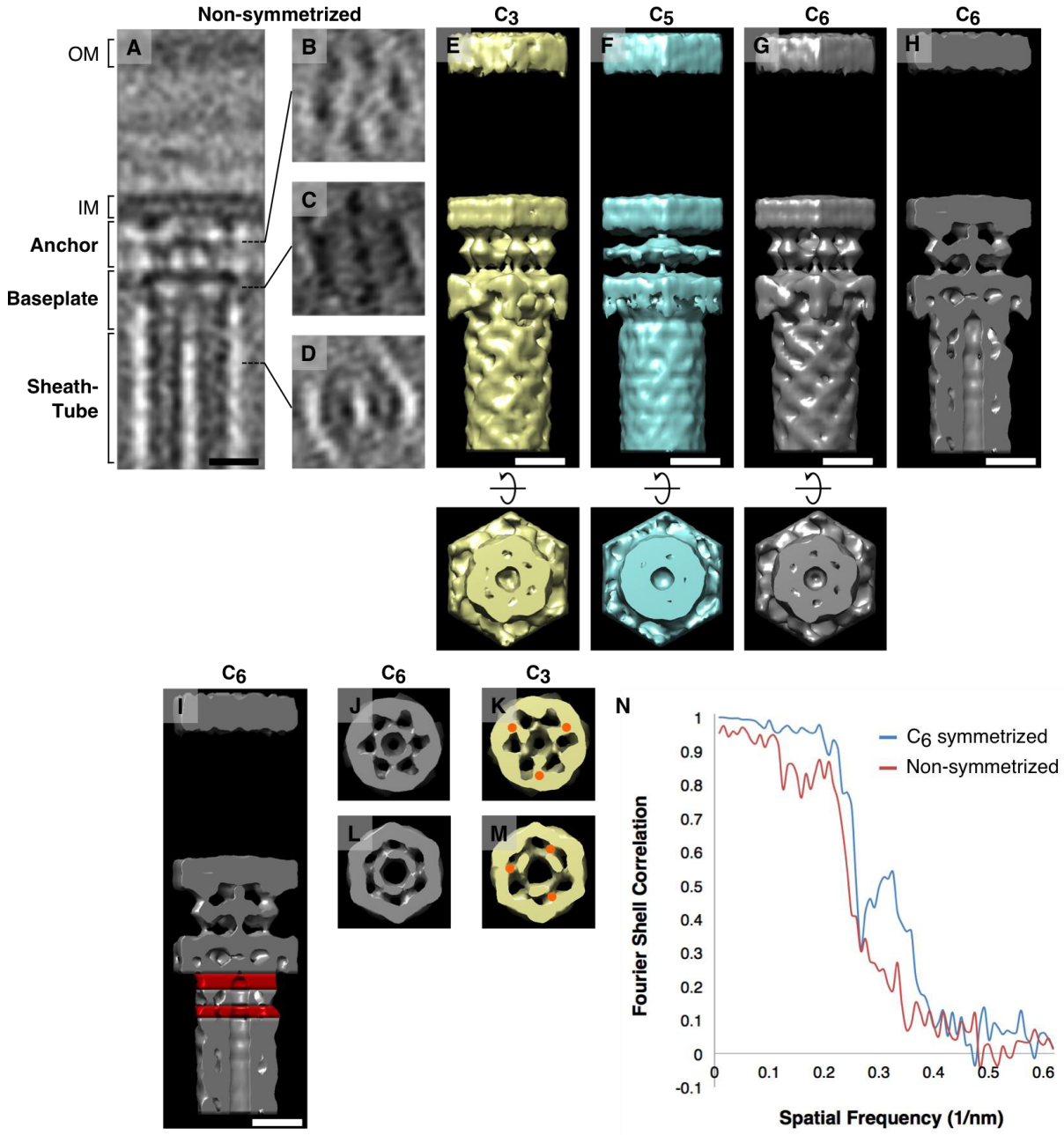

Fig. S2: The *Amoebophilus* T6S apparatus is mostly six-fold symmetric.
(**A-D**) Non-symmetrized version of the extended conformation average shown in Fig. 2A. Shown are 0.81-nm longitudinal (A) and perpendicular (B-D) slices. Similar reconstructions were obtained by starting averaging using different random subvolumes as a first reference (not shown). Rotational six-fold (C6) symmetry was observed in baseplate and anchor (B/C). The tails (D) of phages and canonical T6SS were reported previously having C6-symmetry (*41*, *42*). "OM", outer membrane; "IM", inner membrane.
(**E-H**) Models of C3-, C5-, and C6-symmetrized averages derived from the average shown in (A-D). Overall, the C6 version showed the strongest reinforcement of densities.

The C5-version showed smearing of most densities. The C3 version showed overall C6-symmetry.
(**I-M**) Few densities in the baseplate module showed specific reinforcement in the C3-symmetrized version. Shown is a longitudinal inside view (I) of the model shown in (H). The perpendicular views of the C3 and C6 versions of the volumes indicated in red are shown in (J-M). C3-symmetric densities are indicated by orange discs. Note that densities that would indicate a major cell-envelope spanning complex were not seen in any average.
(**N**) Fourier shell correlation curves show the improvement of resolution of the C6-symmetized average compared to the non-symmetrized version.
Bars: 10 nm.

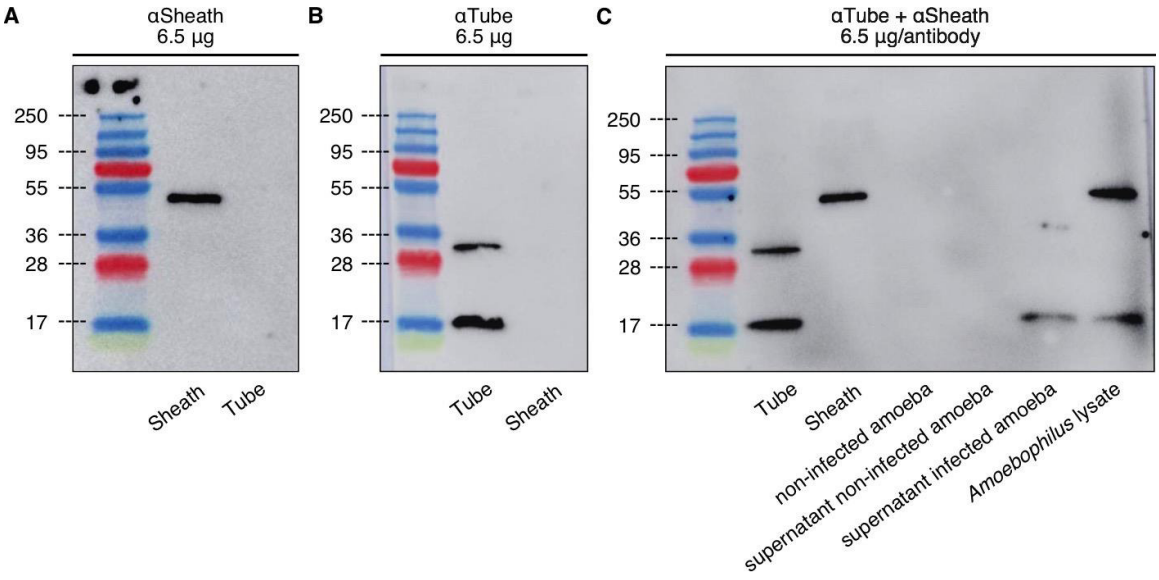

Fig. S3: The *Amoebophilus* T6S inner tube is secreted into extracellular space.
(**A/B**) Western blots using polyclonal antibodies that were raised against inner tube and sheath proteins showed specific signals for recombinant sheath (55 kDa, 15 ng) and tube (17 kDa, 15 ng), respectively.
(**C**) Western blots using a mixture of tube and sheath antibodies detected only tube but no sheath protein in the supernatant of an amoeba culture infected with *Amoebophilus*, indicating that the tube but not sheath was translocated into extracellular space. No signals were obtained from non-infected amoebae and supernatant of non-infected amoebae. Tube and sheath were detected in an *Amoebophilus* lysate. The molecular weights of the markers are indicated in kDa.

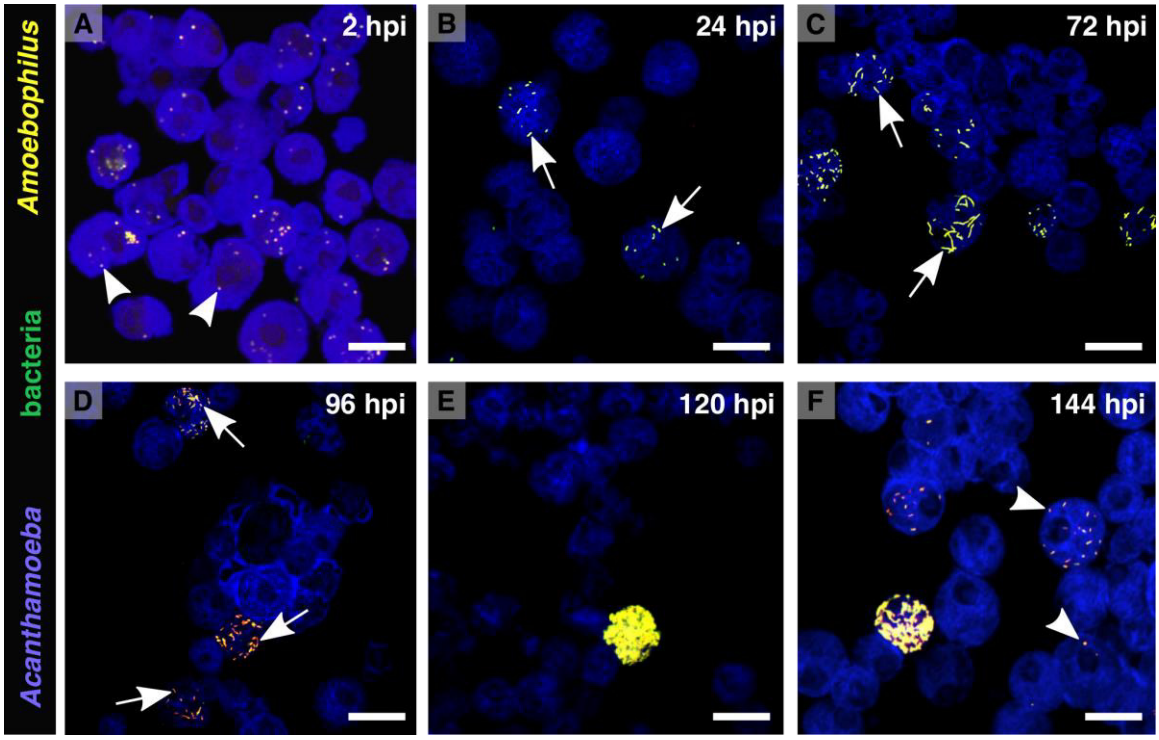

Fig. S4: The *Amoebophilus* life cycle lasts approximately 144 h and cells undergo morphological differentiation.
(**A-F**) Cells were labeled by FISH using three different probes. *Amoebophilus* was specifically detected using Aph1180-Cy3 probe (*10*). An unspecific bacterial probe (EUB338-Fluos) (*26*) was used to identify potential bacterial contaminants. Probe EUK516-Cy5 was used to identify amoebae (*26*). Coccoid amoebophili (white arrowheads) were found inside amoebae at 2 hpi (A). Rod-shaped amoebophili (white arrows) were observed starting at 24 hpi (B/C). At 120 hpi, amoebae were completely filled with amoebophili (E). At 144 hpi, amoebae in early infection stages were observed, indicating the start of a second round of infection (F). Bars: 10 µm.

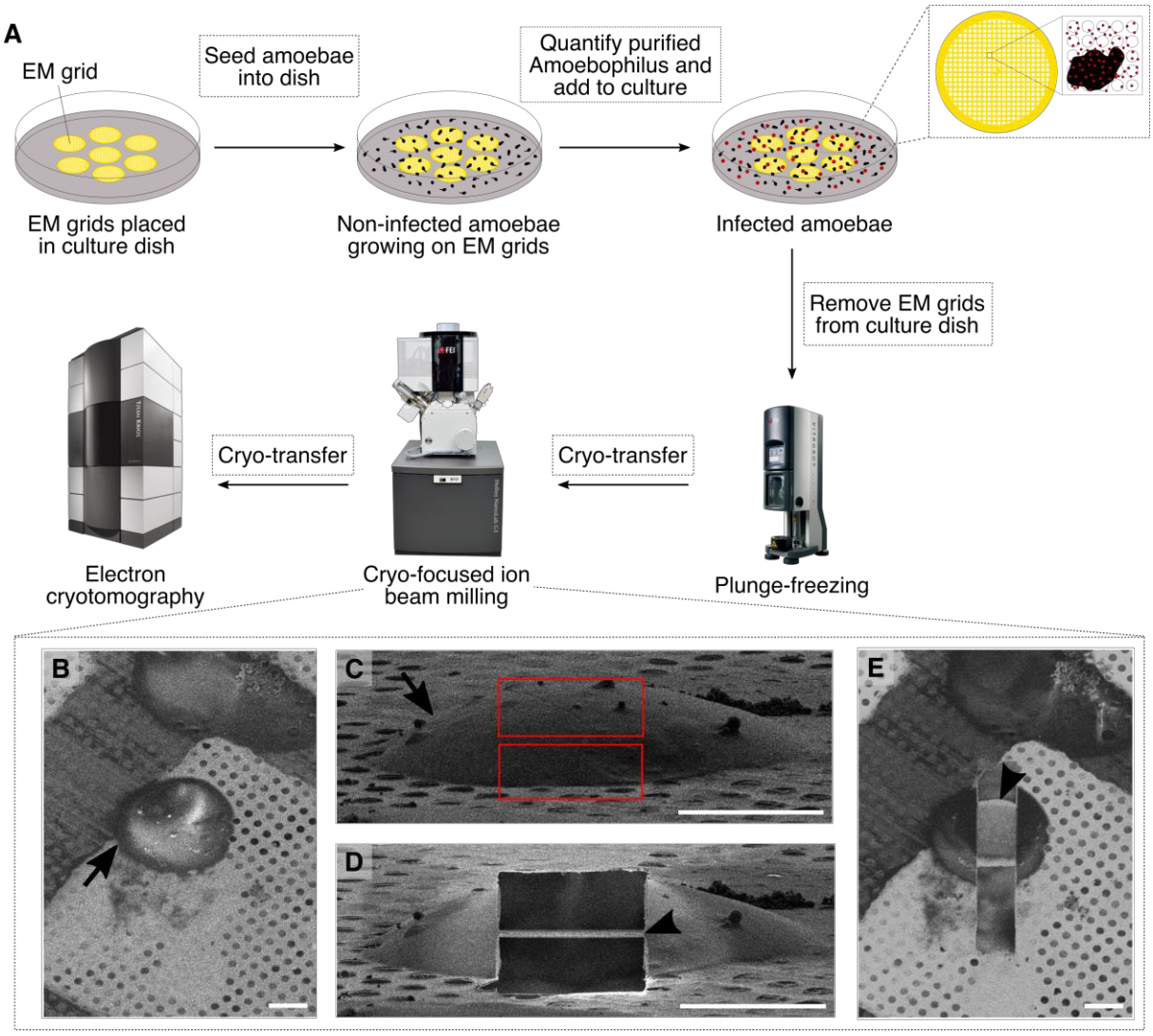

Fig. S5: Workflow for imaging bacteria inside their host by ECT.
(**A**) The schematic shows the major steps including culturing of eukaryotic cells on EM grids (yellow), infecting cells (black) with bacteria (red), plunge-freezing the grids, sample thinning by cryo-focused ion beam (FIB) milling, and ECT imaging.
(**B-E**) Shown are examples of the steps to prepare lamellae by cryo-FIB milling that are thin enough to be subsequently imaged by ECT. A target cell (arrow) is first localized in top view by scanning EM (B). The same cell (arrow) is then imaged at an angle by the FIB, and areas for milling (indicated by rectangles) are specified (C). After milling, the remaining lamella (arrowheads) is inspected by the FIB (D) and by scanning EM from top (E). See also Methods. Bars: 10 µm.

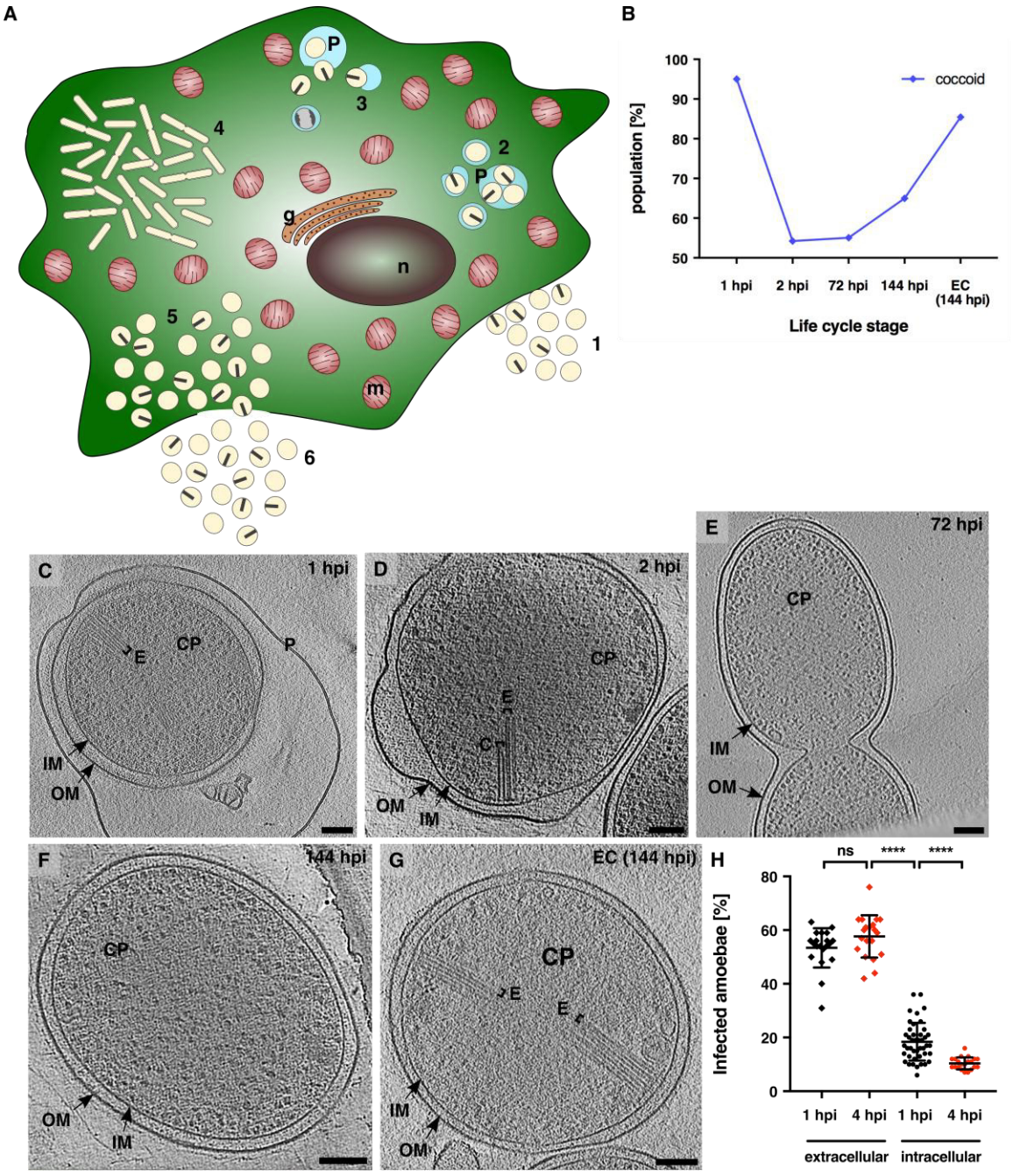

Fig. S6: The *Amoebophilus* developmental and infection cycle in *Acanthamoeba*. (**A**) Shown is a schematic that was established by the integration of FISH data and ECT of cryo-FIB milled samples. The developmental cycle comprises the stages uptake (1), phagosome residence (2), phagosome escape (3), differentiation into rod shaped cells and replication (4), re-differentiation into coccoid cells (5), and exit (6). “g”, golgi; “P”, phagosome; “n”, nucleus; “m”, mitochondrion; yellow, amoebophili; grey, digested amoebophili. T6S arrays (indicated as grey bars) were preferentially expressed in the infectious coccoid stage.

(**B**) The quantification of morphological states (coccoid and rod-shaped) observed throughout the *Amoebophilus* life cycle indicated that cells are replicating after escaping into the cytoplasm, supported by fig. 3E and the fact that rod shaped or dividing cells were never seen inside phagosomes. n^{1hpi}=104, n^{2hpi}=118, n^{72hpi}=218, n^{144hpi}=337, $n^{EC(144\ hpi)}$=55.
(**C-G**) Examples of intracellular (C-F) and extracellular (G) amoebophili purified at different infection stages (hpi indicated). At 1 hpi, 39 % of amoebophili were inside phagosomes ("P") (C; also fig. 3E). At 2 hpi, most amoebophili were not inside a phagosome, the fraction of cells harboring T6S structures was lower, and the rate of contracted structures was higher (D). Only 5 % of the analyzed rod shaped/dividing amoebophili harbored T6S structures (E). At 144 hpi, T6S structures were only found in 7 % of the cells (F), while in the extracellular (EC) population 58 % of the cells had T6S arrays (G). "OM", outer membrane; "IM", inner membrane; "E", extended T6SS; "C", contracted T6SS. Shown are 12-nm slices through cryotomograms. Bars: 100 nm.
(**H**) To test whether T6S gene expression levels would correlate with infectivity (i.e. the potential to infect new host cells and survive intracellularly), amoebae were infected with extracellular (high T6S expression) and late stage intracellular amoebophili (low T6S expression). Intracellular amoebophili display a 3-fold decreased infectivity (measured as the percentage of infected amoebae) at 1 hpi, compared to the extracellular stage (**** $p < 0.0001$; not significant, ns; $n^{intra1hpi}$=2996; $n^{intra4hpi}$=2510; $n^{extra1hpi}$=2166; $n^{extra4hpi}$=2442). Data are displayed as mean and standard deviation.

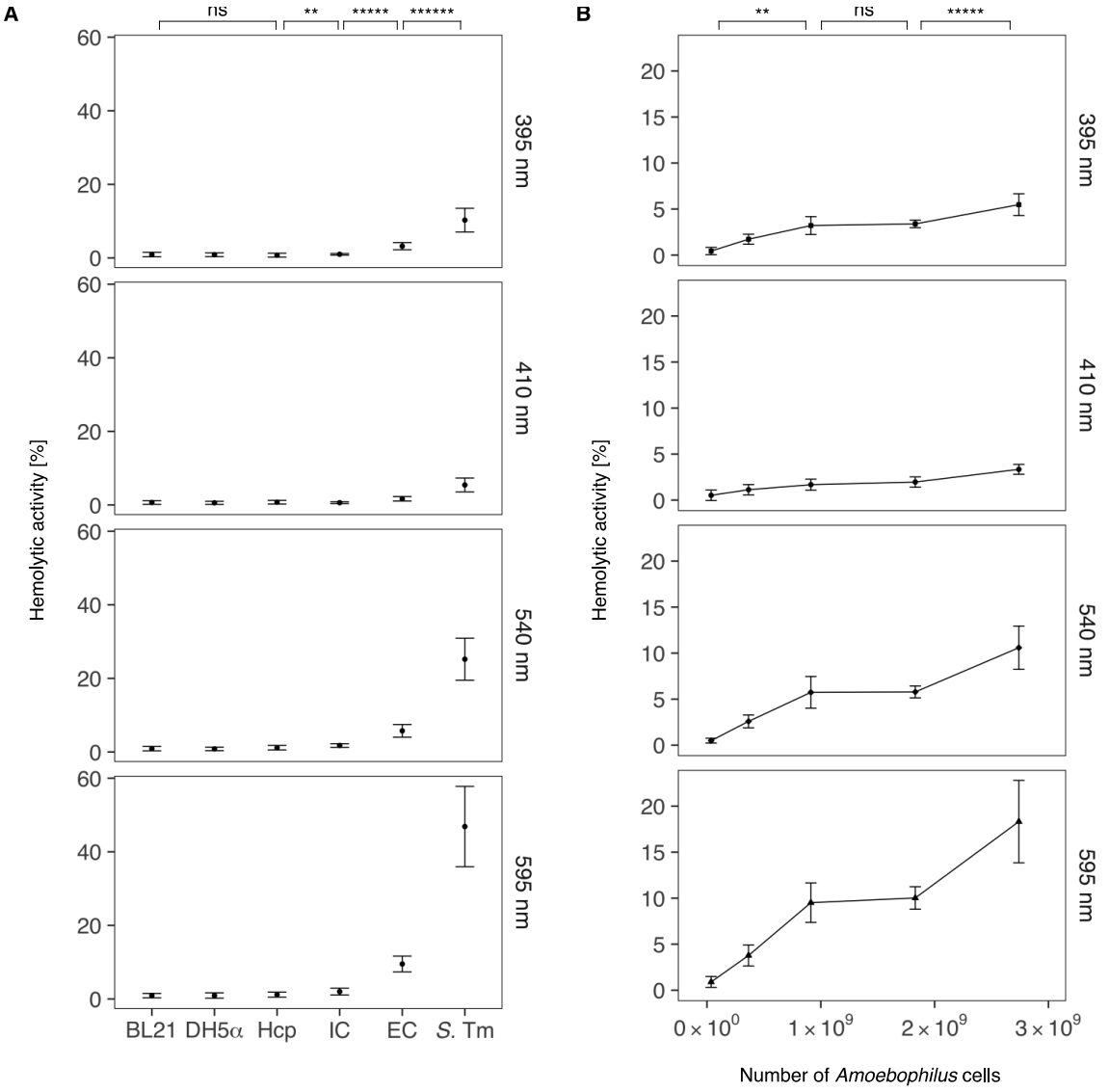

Fig. S7: Extracellular amoebophili (144 hpi) show hemolytic activity.
Different oxidation states of hemoglobin were photometrically measured (wavelengths indicated) as an indicator for red blood cell lysis (*35*).
(**A**) Extracellular amoebophili (EC) displayed a 5-fold increase in hemolysis compared to intracellular amoebophili (IC, 68 hpi) and a 10-fold increase compared to the negative control organisms *E. coli* BL21 (BL21), and *E. coli* DH5α (DH5α), and recombinant Hcp (no lysis expected (*36*)). *Salmonella* Typhimurium strain SL1344 (*S.* Tm) was used as a positive control organism (** $p < 0.01$; ***** $p < 0.00001$; ****** $p < 0.000001$; not significant, ns; $n^{BL21}=24$; $n^{DH5\alpha}=24$; $n^{Hcp}=24$; $n^{IC}=16$; $n^{EC}=40$; $n^{S.Tm}=24$). The 5-fold difference in hemolytic activity between EC and IC suggests an involvement of T6S arrays in the lysis process (only 5 % of ICs harbor T6S arrays).
(**B**) Hemolytic activity of *Amoebophilus* increases with cell number. Extracellular amoebophili were used at MOIs 1, 10, 25, 50 and 75 (** $p < 0.01$; ***** $p < 0.00001$; not significant, ns; $n^{MOI1}=20$; $n^{MOI10}=20$; $n^{MOI25}=40$; $n^{MOI50}=20$; $n^{MOI75}=20$).

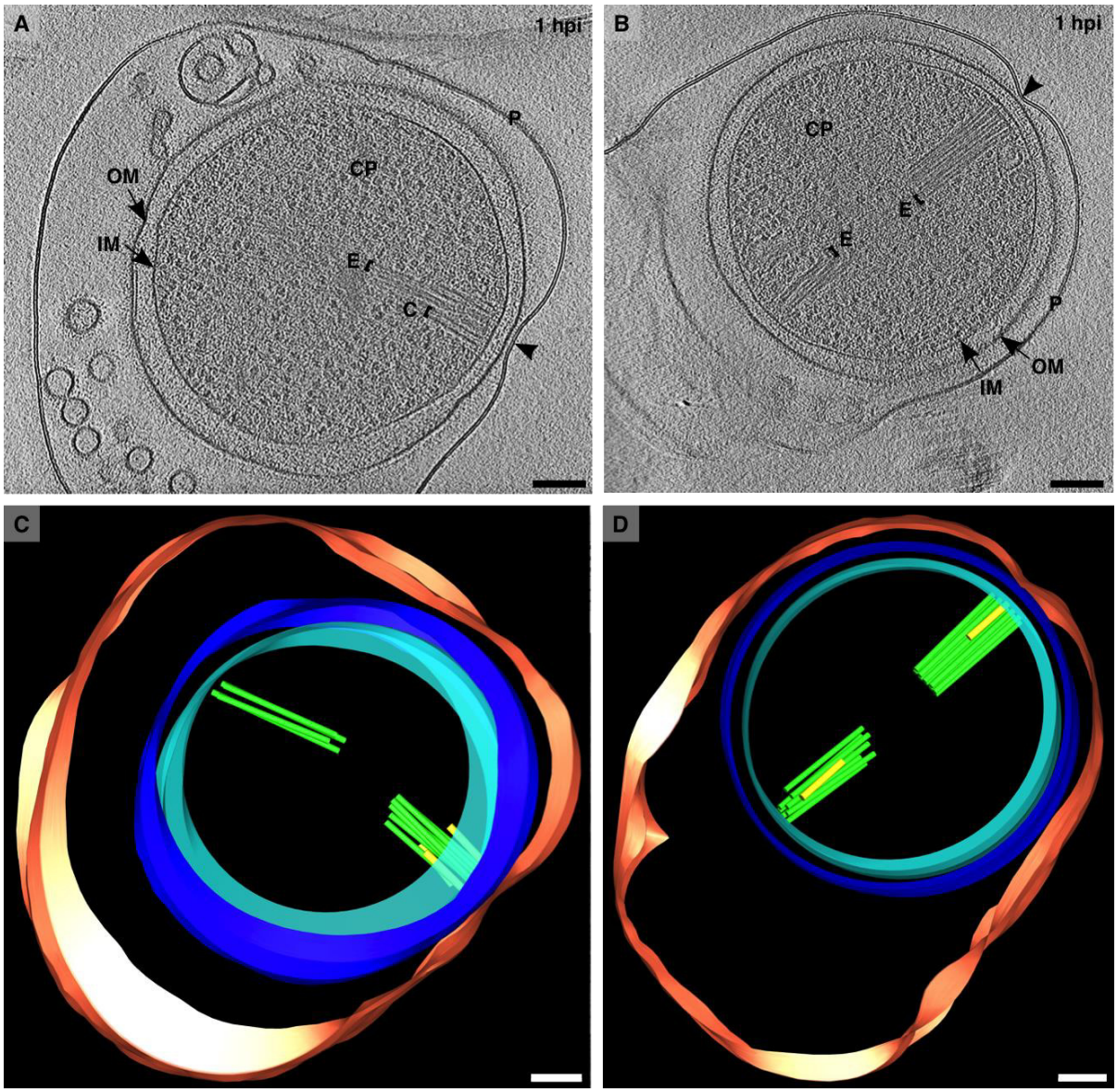

Fig. S8: Contact sites between phagosome membrane and outer membrane co-localize with T6S arrays.
(**A-D**) Shown are further examples of amoebophili inside phagosomes. Anytime a contact site between a phagosome membrane and the *Amoebophilus* outer membrane was detected, the site coincided with a T6S array (with at least one contracted structure) in the exact same location (arrowheads). Shown are 11-nm slices through cryotomograms (A/B) and the respective models (C/D). "P"/red, phagosome membrane; "OM"/blue, outer membrane; "IM"/cyan, inner membrane; "CP", cytoplasm; "E"/green, extended T6SS; "C"/yellow, contracted T6SS. Bars: 100 nm.

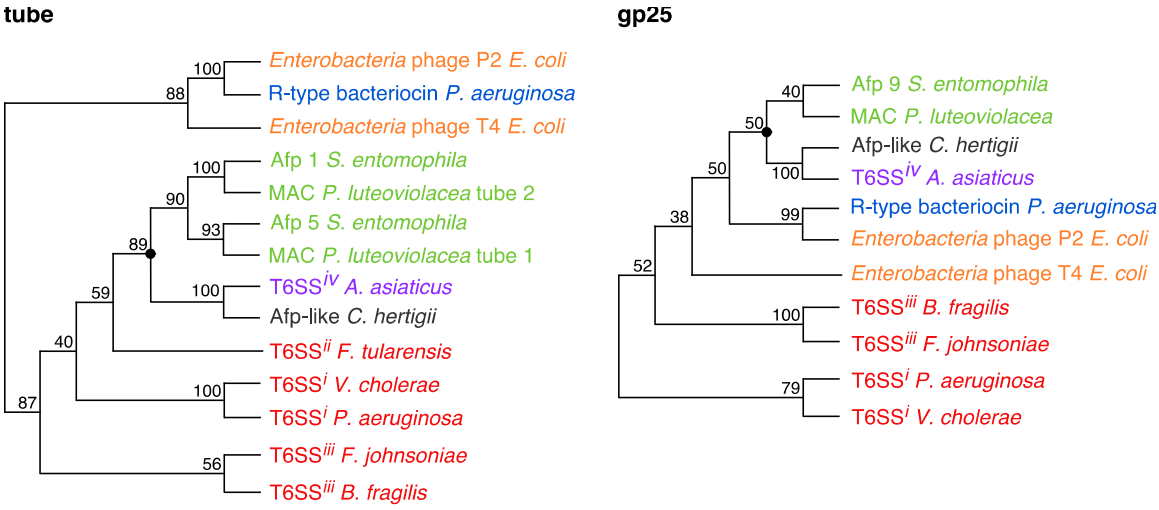

Fig. S9: Phylogenetic analyses of CIS tube and gp25 homologues.
Both trees show that (like for the sheath protein in fig. 4A) the *Amoebophilus* T6S sequence forms a stable monophyletic group with sequences from the eCIS of Afp and MAC, and with a sequence from a *Cardinium* gene cluster with unknown structure/function. This node (marked) was stable in all calculated trees using different treeing methods. Bootstrap supports are indicated at nodes.

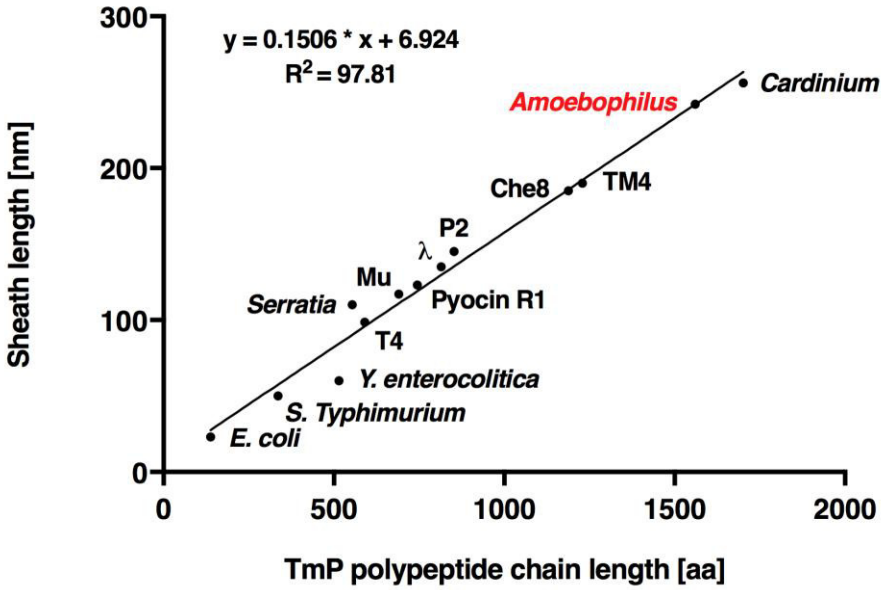

Fig. S10: A tape measure protein (TmP) regulates the sheath length in *Amoebophilus* T6SS.
Shown is a plot of extended sheath length over the number of amino acids (aa) of the respective TmP homologue. The length of *Amoebophilus* sheath (242 nm) fits well with the polypeptide length of Aasi_1806 (1561). The figure was adapted from (*22*). The following assemblies and corresponding TmPs were included in this figure: T4 phage/gp29, *S. entomophila*/Afp14, lambda phage/gpH, P2 phage/gpT, pyocin R1/ORF20, *Amoebophilus*/Aasi_1806, *Cardinium*/Cahe_0118, *E. coli*/EscP, *S.* Typhimurium/InvJ, *Y. enterocolitica*/YscP, Che8 *Mycobacterium* phage/gp14 and TM4 *Mycobacterium* phage/gp17. The length of *Cardinium* sheath was estimated from images in (*17*).

Table S1: Mass spectrometry analysis of the sheath preparation of *Amoebophilus*.

Locus tag *Amoebophilus**	Molecular weight [kDa]	Total unique peptide count	Annotation
Aasi_1074	55	66	Phage tail sheath
Aasi_0557	145	27	Phage baseplate protein
Aasi_1080	66	18	VgrG-spike protein
Aasi_1083	97	15	Afp12-like protein
Aasi_0556	28	13	Afp-like protein
Aasi_1079	38	10	Afp7-like protein
Aasi_1075	18	9	Afp-like protein
Aasi_1076	16	6	Afp-like protein
Aasi_1806	180	5	Afp14-like protein
Aasi_1073	33	4	Afp-like protein
Aasi_1072	22	3	Afp16-like protein
Aasi_0563	126	2	Phage baseplate protein

*Only proteins assigned to the *Amoebophilus* Afp-like gene cluster are shown. All displayed proteins were identified with a probability of 100 %.

Table S2: Relative quantification of sheath (Aasi_1074) mRNA at different life cycle stages of *Amoebophilus.* A housekeeping gene encoding for the beta subunit of the RNA polymerase (*rpoB*, Aasi_1396) was used for normalization.

Life cycle stage	Mean ratio of Cq value (Aasi_1074 relative to Aasi_1396)	Standard deviation	Fold increase*	Standard deviation
Extracellular	10.72	0.87	230.7	18.7
12 hpi	0.20	0.04	4.4	0.8
68 hpi	0.05	0.01	1.0	0.3
140 hpi	1.38	0.04	29.6	0.8

*relative to mRNA level at the intracellular, replicative stage at 68 hpi.

Table S3: Similarities (PSI-BLAST Expect [E] values) of three *Amoebophilus* core components with relatives from other CIS.

E-value	***Amoebophilus* T6S components**		
CIS	**Baseplate gp25 (Aasi_1082)**	**Sheath (Aasi_1074)**	**Tube (Aasi_1077)**
Cardinium Afp-like	2.00E-45	0.00E+00	6.00E-37
P. luteoviolacea MAC	1.00E-18	1.00E-72	2.00E-03 4.00E+00
S. entomophila Afp	2.00E-16	2.00E-54 6.00E-56 1.00E-41	3.00E-07 1.00E-05
Enterobacteria phage T4	1.00E-08	1.00E-10	2.00E+00
Enterobacteria phage P2	3.00E-05	6.00E+00	-
P. aeruginosa R-type bacteriocin	3.00E-07	3.00E-07	4.70E+00
P. aeruginosa T6SS[i]	-	4.60E+00 9.60E+00	-
V. cholerae T6SS[i]	-	1.60E-01 4.10E+00	1.60E-02
F. tularensis T6SS[ii]	-	- -	-
F. johnsoniae T6SS[iii]	4.00E-05	- 7.00E-03	-
B. fragilis T6SS[iii]	7.00E-06	- 4.30E-01	2.00E+00
Locus tags[a]			
Cardinium Afp-like	CAHE_0761	CAHE_0458	CAHE_0461
P. luteoviolacea MAC	JF50_12705	JF50_12675	JF50_12685 JF50_12680
S. entomophila Afp	Afp9	Afp2 Afp3 Afp4	Afp1 Afp5
Enterobacteriophage T4	gp25	gp18	gp19
Enterobacteriophage P2	gpW	FI	FII
P. aeruginosa R-type bacteriocin	WR2	FIR2	FIIR2
P. aeruginosa T6SS[i]	PA0087	PA0083 PA0084	PA1512
V. cholerae T6SS[i]	VC_A0109	VC_A0107 VC_A0108	VC_A0017
F. tularensis T6SS[ii]	-	FTT_1359c FTT_1358c	FTT_1355
F. johnsoniae T6SS[iii]	Fjoh_3263	Fjoh_3267 Fjoh_3266	Fjoh_3262
B. fragilis T6SS[iii]	BF9343_1932	BF9343_1942 BF9343_1941	BF9343_1935

[a]Locus tags are derived from *Amoebophilus asiaticus* 5a2, *Cardinium hertigii* strain *c*Eper1, *P. luteoviolacea* strain HI1, *S. entomophila* plasmid pADAP, *Enterobacteria* phages P2 and T4, R-type bacteriocins, *P. aeruginosa* PAO1, *V. cholerae* ATCC 39315, *F. tularensis* SCHU S4, *F. johnsoniae* UW101 and *B. fragilis* NCTC 9343 (NCBI accessions NC_010830.1, NC_018605.1, NZ_JWIC01000006.1, NC_002523.4, NC_001895.1, NC_000866.4, NC_002516.2, NZ_CP016324.1, NC_006570.2, NC_009441.1, NC_003228.3). If paralogs exist only one was indicated.

Table S4: Genes of the *Amoebophilus* Afp-like gene cluster and detected homologies with components of phages/CIS.

Orthologs in different species[a]					Putative function
Amoebophilus	***S. entomophila***	***Cardinium***	**Bacteriophage**	**T6SS (Reference[b])**	
Aasi_0556	Afp-like	CAHE_0036	gp48	-	Baseplate/tail tube
Aasi_0557	Afp11	CAHE_0037	gp6	TssF[c] (*13*)	Baseplate wedge
Aasi_0563	-	CAHE_0617	gpD (gp27)	-	Baseplate/spike
Aasi_0565	-	CAHE_0837	gpX (gp53)	-	Baseplate wedge
Aasi_1068	-	-	Rz	-	Endopeptidase
Aasi_1072	Afp16	CAHE_0456	gp15	-	Tail terminator protein
Aasi_1073	Afp-like	CAHE_0457	-	-	Unknown
Aasi_1074	Afp2, Afp3, Afp4	CAHE_0458	gp18	TssBC (*24*)	Outer sheath
Aasi_1075	Afp-like	CAHE_0459	-	-	Unknown
Aasi_1076	Afp-like	CAHE_0460	-	-	Unknown
Aasi_1077	Afp1, Afp5	CAHE_0461	gp19	Hcp (*24*)	Tail tube
Aasi_1078	Afp-like	CAHE_0462	-	-	Unknown
Aasi_1079	Afp7	CAHE_0463	gpU (gp54)	-	Baseplate/tail tube
Aasi_1080	Afp8	CAHE_0763	gp5	VgrG (*24*)	Spike
Aasi_1081	Afp-like	CAHE_0762	gp5.4	PAAR (*14*)	Spike tip
Aasi_1082	Afp9	CAHE_0761	gp25	TssE (*24*)	Baseplate wedge
Aasi_1083	Afp12	CAHE_0760	gp6 (gp7[d])	TssF (*13*) (TssG[d])	Baseplate wedge
Aasi_1806	Afp14	CAHE_0118	gp29	-	Tape measure protein

[a]Locus tags are derived from *Amoebophilus asiaticus* 5a2, *S. entomophila* plasmid pADAP, *Cardinium hertigii* strain *c*Eper1, *P. aeruginosa* PAO1, *Enterobacteria* phage P2 and T4 (NCBI accession NC_010830.1, NC_002523.4, NC_018605.1, NC_002516.2, NC_001895.1, NC_000866.4).
[b]Homologies between bacteriophage and T6S components are displayed and were described as indicated.
[c]TssA was suggested as an alternative in (*43*).
[d]Aasi_1083/Aasi_0557/gp6/gp7 homologies are discussed in the main text.

Table S5: A PSI-BLAST search for T6SS^{iv}-like gene clusters (based on the presence of homologues of sheath, tube and baseplate [gp25]) detected hits with high probabilities in many diverse bacteria. Shown are two representatives of each taxonomic group. For comparison, T6SS^{i} sheath (TssBC) from *P. aeruginosa* PAO1 results in much lower E-values (4.6E+00 and 9.6E+00, respectively).

Taxonomic group	Species	Accession number	E-Value (sheath, Aasi_1074)
Alphaproteobacteria	*Aestuariivita atlantica*	WP_050531564	1E-121
Alphaproteobacteria	*Dinoroseobacter shibae*	WP_012179131	9E-117
Betaproteobacteria	*Rhizobacter* sp. *Root1221*	WP_056669399	2E-141
Betaproteobacteria	*Derxia gummosa*	WP_028311256	2E-139
Gammaproteobacteria	*Ca.* Tenderia electrophaga	ALP53857	4E-145
Gammaproteobacteria	*Vibrio maritimus*	WP_042497655.1	9E-137
Deltaproteobacteria	*Desulfoluna spongiiphila*	SCY15357	6E-145
Deltaproteobacteria	*Pelobacter propionicus*	WP_011734321	4E-140
Bacteroidetes	*Sporocytophaga myxococcoides*	WP_045466009	4E-143
Bacteroidetes	*Algoriphagus marincola*	WP_026965902	4E-139
Cyanobacteria	*Moorea producens*	WP_008186241	2E-117
Cyanobacteria	*Pseudanabaena* sp. PCC 7367	WP_015165306	3E-97

Movie S1
Electron cryotomography of an *Amoebophilus* cell with T6S arrays. Shown are cryotomographic slices and a model of the cell shown in Fig. 1A-D.

Movie S2
Subtomogram average of extended *Amoebophilus* T6S structures. Shown are longitudinal and perpendicular cryotomographic slices of the average shown in Fig. 2A.

Movie S3
Density map of an averaged extended *Amoebophilus* T6S structure. Shown are different views of the model shown in Fig. 2C.

Movie S4
Subtomogram average of contracted *Amoebophilus* T6S structures. Shown are longitudinal and perpendicular cryotomographic slices of the average shown in Fig. 2L.

Movie S5
Density map of an averaged contracted *Amoebophilus* T6S structure. Shown are different views of the model shown in Fig. 2M.

Movie S6
Morph between the density maps of averaged extended and contracted *Amoebophilus* T6S structures. Shown are the models shown in Fig. 2C/M.

Movie S7
Cryotomogram of a cryo-FIB milled infected amoeba cell at 0.25 hpi. Shown are slices through the tomogram shown in Fig. 3A.

Movie S8
Cryotomogram of a cryo-FIB milled infected amoeba cell at 0.5 hpi. Shown are slices through the tomogram shown in Fig. 3B.

Movie S9
Cryotomogram of a cryo-FIB milled infected amoeba cell at 0.75 hpi. Shown are slices through the tomogram shown in Fig. 3C.

Movie S10
Cryotomogram of a cryo-FIB milled infected amoeba cell at 2 hpi. Shown are slices through the tomogram shown in Fig. 3D.

Movie S11
Electron cryotomography of an *Amoebophilus* cell inside a phagosome. Shown are slices through the tomogram shown in Fig. 3G and the corresponding model shown in Fig. 3H.